Self-shielding Effect of Double Heterogeneity
for Plutonium Burner HTGR Design

Y. Fukaya*, M. Goto, and H. Ohashi

Sector of Fast Reactor and Advanced Reactor Research and Development

Japan Atomic Energy Agency (JAEA)

4002 Narita-cho, Oarai-machi, Higashiibaraki-gun, Ibaraki 319-1395, Japan

*E-mail: fukaya.yuji@jaea.go.jp

Phone: +81-29-267-1919-6514

Fax: +81-29-266-7703

Total number of Pages: 14

Total number of Tables: 8

Total number of Figures: 25

Abstract

The investigation on self-shielding effect of double heterogeneity for plutonium burner High Temperature Gas-cooled Reactor (HTGR) design has been performed. Plutonium burner HTGR designed in the previous study by using the advantage of double heterogeneity to control excess reactivity. In the present study, the mechanism of the self-shielding effect is elucidated by the analysis of burn-up calculation and reactivity decomposition based on exact perturbation theory. As a result, it is revealed that the characteristics of burn-up reactivity are determined by resonance cross section peak at 1 eV of Pu-240 due to the surface term of background cross section, this is, the characteristics of neutron leakage from fuel lump and collision to a moderator. Moreover, significant spectrum shift is caused during the burn-up period, and it enhances reactivity worth of Pu-239 and Pu-240 in EOL.

KEYWORDS: plutonium burner HTGR, double heterogeneity, self-shielding effect

1. Introduction

In Japan, surplus plutonium is concerned from the viewpoint of nuclear proliferation. In this context, plutonium burner High Temperature Gas-cooled Reactor (HTGR) was proposed by Japan Atomic Energy Agency (JAEA) (Fukaya, et al. 2014), and has been developed as national project offered by Ministry of Education, Culture, Sports, Science and Technology (MEXT) with the cooperation of Japanese research institute, university, and makers, such as JAEA, the University of Tokyo, Fuji Electric Co. Ltd., and Nuclear Fuel Industries Ltd. (Goto, et al. 2015). In the conceptual study (Fukaya, et al. 2014), it is found that excess reactivity can be reduced by controlling self-shielding effect due to double heterogeneity in the core design without reduction of achievable burn-up. Especially for the plutonium fueled reactor, the self-shielding effect is significant because of the large cross sections of plutonium nuclides. The plutonium burner HTGR employs diluted fuel kernel by the chemically inert matrix to enhance the proliferation resistance of plutonium fuel. The plutonium inventory is limited from the viewpoint of neutron moderation. In this condition, a certain amount of plutonium can be assigned the density in the diluted fuel kernel or the number of Coated Fuel Particles (CFPs). In the plutonium burner HTGR design, the excess reactivity can be reduced by weakening the double heterogeneity with the design of the low-density fuel kernel and an increased number of CFP.

In the present study, to elucidate the mechanism of the change on the self-shielding effect, burn-up calculation and reactivity decomposition calculation is performed. The plutonium burner HTGR concept and the excess reactivity suppressed design is described in Section 2. The calculation method is described in Section 3. The calculation result and consideration are described in Section 4.

2. Concept of plutonium burner HTGR and excess reactivity suppression

The plutonium burner HTGR is designed based on commercial HTGR with the output of 600MWt named GTHTR300 (Yan, et al. 2003). Figure 1 shows the core geometry of the reactor core, and the major specifications are listed in Table 1. The fuel region should be increased from the original design from the viewpoint of neutron moderation as shown in Fig1. The plutonium is diluted by Yttria-Stabilized Zirconia (YSZ), which is chemically inert, to enhance the proliferation resistance. By this treatment, the self-shielding effect caused by double heterogeneity can be weakened by diluting the plutonium in the fuel kernel even with the same amount of plutonium in the fuel compact. The fuel specifications is listed in Table 2. Figure 2 shows the criticality change of the plutonium burner HTGR evaluated in the previous study. This is the result of one batch core burn-up preliminary calculation to determine core specifications by MVP code (Nagaya, et al. 2006) with the evaluated nuclear data of JENDL-4.0 (Shibata, et al. 2011). In these calculations, the plutonium inventory is reserved. Therefore, the packing fraction of Coated Fuel Particles (CFPs) increases when the mole fraction of plutonium reduces by diluting by YSZ. The excess reactivity at the Beginning Of Life (BOL) reduces along with the mole fraction reduction without reduction of achievable burn-up. According to the result and manufacturing difficulty, which limits the packing fraction up to 33 % , the representative mole fraction PuO_2 is determined as 30 %.

<Tables 1 and 2, Figs 1 and 2>

3. Calculation Method

3.1 Burn-up Calculation by Monte Carlo Method

In the present study, burn-up calculations are performed by MVP code (Nagaya, et al. 2006), which is neutron transport calculation code based on Monte Carlo method, with the evaluated nuclear data of JENDL-4.0 (Shibata, et al. 2011). In this code, the double heterogeneity can be treated by STatistical Geometry model (STG model) (Murata, et. al 1997). In the STG model, the CFPs are deployed on the neutron flight path according to the

probability specified by users. The reaction rate with CFPs can be controlled by cumulative probability density function named Nearest Neighbor Distribution (NND). NND is defined as the cumulative probability to collision with CFPs along with the neutron flight length. On the other hand, recently, some researches for double heterogeneity with fixed CFP positions is performed (Liu et al. 2015, Ho et al. 2017). One of the researches (Ho et al. 2017) realizes random distribution from the viewpoint of accuracy. However, actual fuel is fabricated by overcoat method (Yoshimura, 1990) to avoid contact between the CFPs. Strictly speaking, the actual CFPs distribution is different from a random distribution. Murata also developed the method to imitate the actual distribution by using the closest random packing with virtually increased particle diameter to consider the overcoat. MCRDF code (Murata, et al. 1996) can evaluate NND for the imitated distribution of the overcoat method. The distribution with the overcoated method can be realized MVP code as well.

On the contrary, the NND for analytical solution of random distribution is implemented for default option of STG model of MVP code. The NND is expressed as follows,

$$NND = 1 - \exp(-\Sigma s) \ , \tag{1}$$

$$\Sigma = N\sigma \ , \tag{2}$$

where:

s: neutron flight length (cm),

N: number density of CFPs (cm^{-3}),

σ: geometric cross section of CFP (cm^2).

Here, the probability density function can be expressed as follows,

$$\frac{dNND}{ds} = \Sigma \exp(-\Sigma s) \ . \tag{3}$$

The eq. (3) shows the collision probability at flight length at neutron flight length s. It is obviously equivalent to corrosion probability of neutron transport problem by regarding σ as

microscopic cross-section and N as atomic number density. The random sampling method of the Monte Carlo method is performed by assigning the uniform random number to the cumulative probability density function and solving the invert equation of eq. (1) to obtain random variable, i.e. neutron flight length s, relating to the random number. The neutron flight length s follows the probability distribution function such as eq. (3). This is the basic principle of random sampling in the Monte Carlo method (Dupree et al. 2004). In this context, the approach of STG model is the essential approach for the Monte Carlo method. The developer of MVP code assessed the accuracy of the STG model for practical HTGR design (Nagaya et al. 2004), and determined it as a default option (Nagaya, 2005). In the present study, the default option is also used.

In addition, the STG model is useful when the fuel matrix region is divided into some regions. Figure 3 shows the calculation model of MVP code to observe the heterogeneity and double heterogeneity effect for spatial shielding effect in burn-up calculations. The fuel compact region is divided into three ring regions, and the fuel kernel of CFPs is divided into three shell regions to equalize the volume of each region.

<Figure 3>

3.2 Generating Reactor Group Constants by Collision Probability Method

To generate reactor group constants, MOSRA-SRAC code (Okumura, 2015) based on collision probability method is employed. That can treat the double heterogeneity by considering microscopic cell region to represent fuel kernel region (Lestie, et al. 1965), and was revised from the previous version of SRAC code (Okumura, et al. 2007) for the treatment of double heterogeneity and resonance cross-section peak, i.e. ultra-fine energy group neutron slowing down calculation (Ishiguro, 1971). In the SRAC code, the double heterogeneity treatment and ultra-fine energy group neutron slowing down calculation are assigned to fast neutron group. The lower boundary is bound to thermal cut-off energy. Both effects are very important to treat double heterogeneity, accurately. Especially for the plutonium fueled reactor,

the lower boundary should be set less than 1eV where the giant resonance peak of Pu-240 exits. However, the thermal cut-off energy is also bound to the upper boundary of up-scattering. The upper boundary of up-scattering should be set approximately 2eV. With SRAC code, plutonium burner HTGR cannot be evaluated accurately. On the contrary, in MOSRA-SRAC code, the lower boundary of the double heterogeneity treatment and ultra-fine energy group neutron slowing down calculation can be set independently from the thermal cut-off energy. Therefore, MOSRA-SRAC code can evaluate the plutonium burner HTGR, accurately. The cell calculation model is shown in Fig.4. However, MOSRA-SRAC code cannot perform burn-up calculations with the double heterogeneity treatment. Therefore, the burn-up composition for the MOSRA-SRAC calculation evaluated by MVP code is used.

<Figure 4>

3.3 Reactivity Decomposition by Exact Perturbation Theory

With the reactor group constant generated by MOSRA-SRAC code, the decomposed reactivity is evaluated by exact perturbation theory (Cacuci 2010). It is derived without approximation from the two criticality equations of the adjoint equation in the reference state and the forward equation in the perturbed state as follows,

$$\rho = \frac{\langle \phi^* \left(-\Delta L + \frac{1}{k'} \Delta P \right) \phi' \rangle}{\langle \phi^* P \phi' \rangle}, \tag{4}$$

where,

ρ: reactivity (-),

ϕ^*: adjoint neutron flux in the reference state (-),

ϕ': neutron flux in the perturbed state ($cm^{-2}s^{-1}$),

ΔL: difference of neutron loss operator between the two states (cm^{-1}),

ΔP: difference of neutron production operator between the two states (cm^{-1}),

P: neutron production operator in the reference state (cm^{-1}),

k': multiplication factor in the perturbed state (-).

The bracket stands for the integration for whole energy and space region. By the exact perturbation theory, the reactivity can be assigned to arbitrary energy and space range by limiting the range of integration. The difference of operators, which are basically composed of macroscopic cross-sections, can be divided into composition related to each nuclide by decomposing the macroscopic cross-sections into products of atomic number density and microscopic cross sections for each nuclide. For the type of reactions, it can be divided into absorption, neutron leakage, scattering, and fission. In this study, the reactivity change for energy is modified to assigned to the energy range where the cross section is perturbed. For scattering and fission reaction, the reactivities can be expressed as follows,

$$\rho_{s,g} = \frac{-\sum_g \phi_g' \sum_{g' \neq g} \delta\Sigma_{s,g \to g'}\left(\phi_g^* - \phi_{g'}^*\right)}{\langle \phi^* P \phi' \rangle}, \tag{5}$$

$$\rho_{f,g}$$

$$= \frac{\frac{1}{k'}\sum_g \phi_g^* \Delta\chi_g \sum_{g'} \upsilon\Sigma_{f,g'}\phi_{g'}' + \frac{1}{k'}\sum_g \Delta\upsilon\Sigma_{f,g}\phi_g' \sum_{g'} \phi_{g'}^*\chi_{g'} + \frac{1}{k'}\sum_g \Delta\upsilon\Sigma_{f,g}\phi_g' \sum_{g'} \phi_{g'}^*\Delta\chi_{g'}}{\langle \phi^* P \phi' \rangle}, \tag{6}$$

where,

$\rho_{s,g}$: reactivity caused by scattering cross section change in the g-th energy group (-),

$\rho_{f,g}$: reactivity caused by fission cross section and/or fission spectrum change in the g-th energy group (-),

$\delta\Sigma_{s,g \to g'}$: change of scattering matrix to slow down from the g-th to g'-th energy group (cm^{-2}),

$\upsilon\Sigma_{f,g}$: production cross section in the g-th energy group (cm^{-2}),

$\Delta\upsilon\Sigma_{f,g}$: change of production cross section in the g-th energy group (cm^{-2}),

χ_g: fission spectrum in the g-th energy group (-),

$\Delta\chi_g$: change of fission spectrum in the g-th energy group (-).

In the present study, the reactivity decomposition calculation is performed by an infinite system. The neutron leakage is evaluated as the product of diffusion coefficient and geometry

8

buckling. To decompose the reactivity, the microscopic cross-section relating to diffusion coefficient is defined as follow,

$$\sigma_{D,i} \equiv 3D^2\sigma_{tr,i} \ , \qquad\qquad (7)$$

where,

$\sigma_{D,i}$: microscopic cross-section relating to diffusion coefficient for i-th nuclide (cm^{-2}),

$\sigma_{tr,i}$: neutron transport microscopic cross-section for i-th nuclide (cm^{-2}).

The summation of the product of the cross-section and atomic number density yield the diffusion coefficient. By using this cross-section, the reactivity caused by neutron leakage can be decomposed for each nuclide.

4. Calculation Result and Consideration

4.1 Spatial Self-shielding Effect

In this section, burn-up calculation is performed by MVP code, and the result is discussed to elucidate the spatial self-shielding effect.

Figures 5-7 show the spatial self-shielding for the heterogeneity and double heterogeneity at BOL. For the heterogeneity, the neutron flux reduces from outside (ring3) to inside (ring1) of a fuel rod. The magnitude becomes approximately 1/3. However, the shape keeps similar figures. For the double heterogeneity, the neutron flux slightly reduces from outside (shell3) to inside (shell1) of fuel kernel for the resonance peak of Pu-240 (1 eV) and Pu-239 (0.3 eV). Therefore, the averaged burn-up characteristics for each region may not be so different with region averaged characteristics.

Figures 7-17 show the difference of burn-up composition for each region from region averaged composition, which is evaluated by treating one burn-up region for the whole fuel kernels. Pu-239, Pu-240, and Pu-241 show the large difference. Pu-239 and Pu-240 increase from region averaged composition along with burn-up by spatial self-shielding effect because of the reduction of the reaction at the energy of the resonance peak. On the contrary, Pu-241 decreases because it is generated by the capture reaction of Pu-240. The spatial effect is the

most significant in the region of ring1-shell1. The difference of Pu-240 is approximately 25% at the burn-up of 600 GWd/t. That is approximately -25% in the region of ring3-shell3. For the fuel composition, the heterogeneity, i.e. ring regions, does not show a significant difference, but the double heterogeneity, i.e. shell regions, shows the significant difference. However, averaged composition for each region shown in Fig. 17 shows a good agreement with the region averaged burn-up composition within 5%. The reactivity difference of the multiple burn-up region model compared with one burn-up region model is shown in Fig. 18. The worth is less than 0.1%Δk/kk', which is negligible, during the burn-up. As a result, it is concluded that spatial self-shielding effect is negligible for plutonium burner HTGR.

<Figs. 5-18>

4.2 Change of Energy Self-shielding Effect

In this section, the reactivity is decomposed by the exact perturbation theory with the result of MOSRA-SRAC calculation and the burn-up composition obtained by MVP code.

Tables 3 and 4 list the reactivity of each reaction at BOL and EOL when the PuO_2 mole fraction of 30 % in reference state changes to 20, 40 and 50 %. The reactivities of absorption and fission are significant. On the contrary, those of leakage and scattering are negligible. Figures 19-24 show the reactivity distribution for neutron energy of each nuclide. At BOL, the reactivities are caused at the energy where the resonance cross-section peak of Pu-239 (0.3 eV), Pu-240 (1 eV) exist. At EOL, the reactivity peak of Pu-241 at 0.3 eV is also observed. For the case with the PuO_2 mole fraction of 20 %, absorption reaction causes negative reactivities, and fission reaction causes positive reactivities because the energy shielding effect is weakened. On the contrary, absorption and fission reactions cause positive and negative reactivates, respectively, for the cases with mole fraction of 40 and 50 %. Thus, reactivity changes are caused at only the energy of resonance cross section peak.

Tables 5 and 6 list the reactivity of each nuclide at BOL and EOL when the PuO_2 mole fraction of 30 % in reference state changes to 20, 40 and 50 %, and table 7 lists number

density for averaged fuel cell at BOL and EOL. The reactivity worth of Pu-239 remains in EOL even with the significant inventory consumption. The characteristics depend on neutron flux and are described later. The worth of Pu-240 reduces due to the inventory consumption, and the worth of Pu-241 increases due to the Pu-240 conversion. The Pu-240 causes negative reactivity with weakened double heterogeneity, and Pu-239 and Pu-240 cause positive reactivity. As a result, the reactivity change among the design with various PuO$_2$ mole fraction reduces. This is the reason why the burn-up reactivity reduces with lower PuO$_2$ mole fraction design. For the excess reactivity control in BOL, the Pu-240 significantly contributes the reactivity change as listed in Table 6. The characteristics also contribute the burn-up reactivity reduction with lower PuO$_2$ mole fraction design via the burn-up composition. These depend on the self-shielding effect of resonance cross section peak of Pu-240 at 1 eV. Here, it is confirmed that the tendency is caused by the weakened double heterogeneity, and it is caused by the larger background cross section according to Bondarenko approach (Bondarenko, 1964) due to the reduced composition of Pu-240 for the lower mole fraction of PuO$_2$.

In Bondarenko approach, the background cross section is expressed as follows,

$$\sigma_{0,n} = \frac{1}{N_n} \sum_{m \neq n} N_m \sigma_{t,m} + \frac{(1-C)\Sigma_e}{N_n} \ , \qquad (8)$$

where:

N_n: atomic number density for m-th nuclide (cm^{-3}),

$\sigma_{0,n}$: background cross section for n-th nuclide (cm^{-2}),

$\sigma_{t,m}$: microscopic total cross section for m-th nuclide (cm^{-2}),

Σ_e: macroscopic escape cross section (cm^{-1}),

C: Dancoff correction factor (-).

Wigner introduced the escape cross section (Wigner, et al. 1955), which is defined as invert of mean chord length, to consider the effect of neutron escape from the fuel lump, and Carlvik applied the Dancoff correction factor to the escape cross section (Carlvik 1966) to consider

the effect of neutron re-entrance to the fuel lump without collision in moderator region. The first term of light hand side of Eq. (8) is called volume term, and the second term is called surface term. Moreover, the macroscopic escape cross section for double heterogeneity problem was introduced by Segev (Segev, 1982) as follows,

$$\Sigma_e = \frac{1}{l} \frac{1}{\frac{1}{\alpha} + \left(\frac{1}{1-c} - 1\right)\beta} \quad , \tag{9}$$

$$\beta = \frac{v_m \Sigma_m}{v_m \Sigma_m + \frac{1/L}{\frac{1}{A} + \frac{1}{1-C} - 1}} \quad , \tag{10}$$

where,

l: mean chord length of the fuel lump (cm),

L: mean chord length of fuel rod (cm),

α: Bell factor of the fuel lump (-),

A: Bell factor of fuel rod (-),

c: Dancof factor of the fuel lump in fuel compact region (-),

v_m: volume fraction of moderator in fuel compact region (-),

Σ_m: macroscopic cross section of moderator in fuel compact region (cm^{-1}).

However, this escape cross section includes all heterogeneity effect. In other words, it is equivalent to $(1-C)\Sigma_e$ in eq (8). The Dancof factor of the fuel lump was introduced by Lane (Lane, et al. 1962) as follows,

$$c = \frac{\lambda}{\lambda + \lambda_f} \quad , \tag{11}$$

where,

λ: mean free path in the moderator (cm),

λ_f: mean free path between fuel lumps (cm).

With the data calculated by MOSRA-SRAC code, the background cross sections are evaluated for Pu-240 at 1 eV and BOL, and listed in Table 8. The energy group from 1.04404eV to 1.07047 eV represents the resonance peak energy. The lower PuO$_2$ mole

fraction case shows a larger background cross section for surface terms. The volume terms are almost same because the difference is caused only by the YSZ nuclides, which are also inert from the viewpoint of nuclear reaction. The escape cross sections increase along with the PuO_2 mole fraction mainly due to the microscopic Dancoff correction, that is $(1 - c)$. The microscopic Dancoff correction is determined in Eq. (11). However, the tendency is inverse compared with the surface term, and inverted by dividing number density in fuel kernel region according to the definition in Eq. (8). Finally, the total background cross section of the lower PuO_2 mole fraction design becomes larger. Those weakened the energy self-shielding of the resonance cross section peak at 1 eV.

Finally, the effect of spectrum change is investigated. Here, importance weighted neutron flux defined as follow,

$$\bar{\phi} = \frac{\phi^* \phi'}{\langle \phi^* P \phi' \rangle} \,,$$

(12)

is evaluated as shown in Fig. 25. The significant spectrum shift, in which the spectra become softer from BOL to EOL, is observed. The flux is directly related to reactivity change with the cross section change according to the definition in Eq. (12). The Maxwellian distribution of the fluxes become twice in EOL. The peak energy is almost same as the resonance cross section peak of Pu-239 and Pu-240. On the other hand, the difference is mere at the energy of 1 eV, where the peak of Pu-241 exists. As a result, the reactivity worth of Pu-239 and Pu-240 are strongly enhanced due to the spectrum shift.

<Tables 3-8>   <Figs. 19-25>

5. Summary

To elucidate the excess reactivity control mechanism by using a change of double heterogeneity for plutonium burner HTGR, Space and energy self-shielding effect of double heterogeneity are evaluated by observing the neutron flux, burn-up compositions, and criticalities. Moreover, reactivity is decomposed quantitively by an exact perturbation method.

13

As a result, the mechanism of the self-shielding effect is found as follows,

➢ The gentle space self-shielding effect is observed inner of fuel compact and fuel kernel. However, the averaged characteristics can be represented by region average solution with enough accuracy both for burn-up composition and criticality.

➢ By comparing between each PuO_2 mole fraction case, the major reactivity is caused at resonance cross section peaks, whose representatives are at 0.3 eV of Pu-239, 1 eV of Pu-240, and 0.3 eV of Pu-241.

➢ The change of self-shielding effect of Pu-240 controls the excess reactivity at BOL, and determined the burn-up reactivity via the burn-up composition.

➢ The characteristics of self-shielding effect of Pu-240 is determined by the surface term of background cross section mainly due to its number density in the kernel region depending on plutonium dilution by YSZ.

➢ Significant spectrum shift causes between BOL to EOL. By the shift, the reactivity worth is significantly enhanced to Pu-239 and Pu-240.

References

Bondarenko, I., 1964. Group constants for nuclear reactor calculations. Consultants Bureau, New York.

Cacuci, D. G., 2010. Handbook of nuclear engineering: Nuclear engineering fundamentals. Springer.

Carlvik, I., 1966. The Dancoff correction in square and hexagonal lattices, Part of Carlvik's PhD thesis. Chalmers University.

Dupree, S. A., Fraley, S. K., 2004. A Monte Carlo primer Volume 2, Plenum Publishers, New York.

Fukaya, Y., Goto, M., Ohashi, H., et al., 2014. Proposal of a plutonium burner system based on HTGR with high proliferation resistance. J. Nucl. Sci. Technol. 51(6), 818-831.

Goto, M., Demachi, K., Ueta, S., 2015. Conceptual study of a plutonium burner high temperature gas-cooled reactor with high nuclear proliferation resistance. Proceeding of GLOBAL 2015. Paris France. Sept. 21-25. 2015, 507-513.

Ho, H. Q., Honda, Y., Goto, M. et al., 2017. Numerical investigation of the random arrangement effect of coated fuel particles on the criticality of HTTR fuel compact using MCNP6, Ann. Nucl. Energ. 103, 114-121.

Ishiguro, Y., 1971. PEACO-II: A Code for Calculation of effective cross section in heterogeneous systems. Japan Atomic Energy Research Institute, JAERI-M 5527.

Lane, R. K., Nordheim, L. W., Sampson, J. B.,1962. Resonance absorption in materials with grain structure. 14, 390-396.

Leslie, D. C., Jonsson, A., 1965. The calculation of collision probabilities in cluster-type fuel elements, Nucl. Sci. Eng., 23, 272-290.

Liu, S., She, D., Liang, J., Wang, K., 2015. Development of random geometry capability in RMC code for stochastic media analysis. Ann. Nucl. Energ. 85, 903-908.

Murata, I., Mori, T., Nakakawa, M., 1996. Packing simulation code to calculate distribution on function of hard spheres by Monte Carlo method: MCRDF. Japan Atomic Energy Research Institute, JAERI-Data/Code 96-016.

Murata, I, Takahashi, A., Mori, T., et al., 1997. New sampling method on continuous energy Monte Carlo calculation for pebble bed reactors. J. Nucl. Sci. Technol. 34(8), 734-744.

Nagaya, Y., Okumura, K., Mori, T., et al.2004. Analysis of the HTR-10 Initial Core with a Monte Carlo Code MVP", Physor 2004, April 25-29, 2004 Chicago, Illinois.

Nagaya, Y., 2005. General purpose Monte Carlo codes for neutron and photon transport calculations based on continuous energy and multigroup methods : MVP/GMVP II, RIST News, 40. [in Japanese]

Nagaya, Y., Okumura, K., Mori, T., 2006. A Monte Carlo neutron/photon transport code MVP 2, Trans. Am. Nucl. Soc. 95, 662-663.

Okumura, K., Kugo T., Kaneko, K., Tsuchihashi, K., 2007. SRAC2006 : A Comprehensive Neutronics Calculation Code System, Japan Atomic Energy Agency, JAEA-Data/Code 2007-004.

Okumura, K., 2015. MOSRA-SRAC: Lattice Calculation Module of the Modular Code System for Nuclear Reactor Analyses MOSRA. Japan Atomic Energy Agency, JAEA-Data/Code 2015-015.

Segev M., 1982. An Equivalence Relation for a Doubly Heterogenous Lattice. Nucl. Sci. Eng. 81, 151-160.

Shibata, K., Iwamoto, O., Nakagawa, T., et al. 2011. JENDL-4.0: A New Library for Nuclear Science and Engineering. J. Nucl. Sci. Technol. 48(1), 1-30.

Yan, X., Kunitomi, K., Nakata, K., et al., 2003. GTHTR300 design and development. Nucl. Eng. Des. 222, 247-262.

Yoshimura, S., Suzuki, N., Kaneko, M., et al. 1990, Production Process and Quality Control System for the HTTR Fuel. Proc. IAEA Specialists Meeting on Behavior of Gas Cooled Reactor Fuel under Accident Conditions, Oak Ridge, USA, 37-42.

Wigner, E., Creutz, E., Jupnik, H., et al. 1955. Resonance absorption of neutrons by spheres. J. Appl. Phys. 26(3), 260-270.

Captions of Tables and Figures

Table 1 Major specifications of plutonium burner HTGR

Table 2 Fuel compositions and packing fractions of plutonium burner HTGR

Table 3 Reactivity of each reaction for various mole fraction compared

with reference case at BOL (Δk/kk')

Table 4 Reactivity of each reaction for various mole fraction compared

with reference case at EOL (Δk/kk')

Table 5 Reactivity of each nuclide in BOL (Δk/kk')

Table 6 Reactivity of each nuclide in EOL (Δk/kk')

Table 7 Number density for averaged fuel cell at BOL and EOL (barn^{-1}cm^{-1})

Table 8 Background cross section and conditions for Pu-240 at 1 eV and BOL

Fig. 1 Core geometry of plutonium burner HTGR

Fig. 2 Excess reactivity suppression by fuel dilution

Fig. 3 Calculation model of MVP code to observe the heterogeneity

and double heterogeneity effect

Fig. 4 Calculation model of MOSRA-SRAC code

Fig. 5 Neutron flux in fuel kernel in ring1 region at BOL

Fig. 6 Neutron flux in fuel kernel in ring2 region at BOL

Fig. 7 Neutron flux in fuel kernel in ring3 region at BOL

Fig. 8 Difference of burn-up composition in ring1-shell1 region

from that of one-region model

Fig. 9 Difference of burn-up composition in ring1-shell2 region

from that of one-region model

Fig. 10 Difference of burn-up composition in ring1-shell3 region

from that of one-region model

Fig. 11 Difference of burn-up composition in ring2-shell1 region

Table 1 Major specifications of plutonium burner HTGR

Items	Design values
Thermal power [MWt]	600
Heavy metal inventory [ton]	1.2
Discharge burn-up [GWd/t]	500
Number of columns [-]	144
Number of batch [-]	4
Number of blocks per columns [-]	8
Number of fuel pins per columns [-]	57
Fuel column height [cm]	105
Fuel rod radius [cm]	1.3
Inner radius of fuel compact [cm]	0.45
Outer radius of fuel compact [cm]	1.2
Packing fraction [%]	-a)
Kernel diameter [μm]	300
Buffer thickness [μm]	150
IPC thickness [μm]	35
SiC thickness [μm]	35
OPC thickness [μm]	40
Kernel density [g/cm^3]	-a)

a) See Table 2.

Y. Fukaya:

Self-shielding Effect of Double Heterogeneity for Plutonium Burner HTGR Design

Table 2 Fuel compositions and packing fractions of plutonium burner HTGR

PuO$_2$ mole fraction (%)	Composition	PuO$_2$ density (g/cm^3)	Packing fraction (%)
20	64Zr-17Y-19Pu	2.46	46.5
30	56Zr-15Y-29Pu	3.63	31.6
40	48Zr-13Y-39Pu	4.77	24.0
50	40Zr-11Y-49Pu	5.87	19.5

※Pu includes MAs.

Y. Fukaya:

Self-shielding Effect of Double Heterogeneity for Plutonium Burner HTGR Design

Table 3 Reactivity of each reaction for various mole fraction compared

with reference case at BOL (Δk/kk')

	Mole frac. = 20%	Mole frac. = 40%	Mole frac. = 50%
Absorption	-4.939E-02	4.447E-02	7.955E-02
Leakage	-2.958E-05	9.597E-06	1.274E-05
Scattering	-2.862E-04	-2.544E-05	-1.280E-04
Fission	2.680E-02	-2.619E-02	-4.684E-02
Total	-2.290E-02	1.826E-02	3.260E-02

Y. Fukaya:

Self-shielding Effect of Double Heterogeneity for Plutonium Burner HTGR Design

Table 4 Reactivity of each reaction for various mole fraction compared

with reference case at EOL ($\Delta k/kk'$)

	Mole frac. = 20%	Mole frac. = 40%	Mole frac. = 50%
Absorption	-4.287E-02	4.174E-02	7.427E-02
Leakage	-4.547E-05	1.729E-05	2.512E-05
Scattering	-7.857E-04	2.404E-04	2.889E-04
Fission	3.654E-02	-3.753E-02	-6.686E-02
Total	-7.161E-03	4.466E-03	7.731E-03

Y. Fukaya:

Self-shielding Effect of Double Heterogeneity for Plutonium Burner HTGR Design

Table 5 Reactivity of each nuclide in BOL (Δk/kk')

	Mole frac. = 20%	Mole frac. = 40%	Mole frac. = 50%
Pu-238	-2.933E-06	8.636E-06	1.349E-05
Pu-239	3.302E-03	-2.480E-03	-3.722E-03
Pu-240	-2.144E-02	1.707E-02	2.995E-02
Pu-241	4.643E-04	-5.109E-04	-8.212E-04
Pu-242	-2.802E-04	2.902E-04	4.927E-04

Y. Fukaya:

Self-shielding Effect of Double Heterogeneity for Plutonium Burner HTGR Design

Table 6 Reactivity of each nuclide in EOL ($\Delta k/kk'$)

	Mole frac. = 20%	Mole frac. = 40%	Mole frac. = 50%
Pu-238	4.018E-05	4.078E-05	4.222E-05
Pu-239	4.238E-03	-3.856E-03	-6.727E-03
Pu-240	-9.519E-03	8.337E-03	1.514E-02
Pu-241	5.599E-03	-6.247E-03	-1.107E-02
Pu-242	-8.294E-04	7.524E-04	1.318E-03

Y. Fukaya:

Self-shielding Effect of Double Heterogeneity for Plutonium Burner HTGR Design

Table 7 Number density for averaged fuel cell at BOL and EOL (barn^{-1}cm^{-1})

	BOL	EOL			
		Mole frac. = 20%	Mole frac. = 30%	Mole frac. = 40%	Mole frac. = 50%
Pu-238	2.547E-07	1.023E-06	1.030E-06	1.029E-06	1.031E-06
Pu-239	9.696E-06	2.400E-06	2.350E-06	2.295E-06	2.255E-06
Pu-240	3.938E-06	2.683E-06	2.836E-06	2.965E-06	3.083E-06
Pu-241	1.427E-06	2.477E-06	2.423E-06	2.350E-06	2.292E-06
Pu-242	9.286E-07	1.496E-06	1.497E-06	1.489E-06	1.486E-06

Y. Fukaya:

Self-shielding Effect of Double Heterogeneity for Plutonium Burner HTGR Design

Table 8 Background cross section and conditions for Pu-240 at 1 eV and BOL

	Mole frac. = 20 %	Mole frac. = 30 %	Mole frac. = 40 %	Mole frac. = 50 %
Volume term (barn)	4.126E+04	4.114E+04	4.108E+04	4.105E+04
Surface term (barn)	2.123E+04	1.766E+04	1.527E+04	1.350E+04
Escape cross section (cm^{-1})	2.402E+01	2.952E+01	3.353E+01	3.649E+01
Microscopic Dancoff correction (-)	2.623E-01	3.435E-01	4.079E-01	4.589E-01
Number density of Pu-240 ($barn^{-1}cm^{-1}$)	1.132E-03	1.672E-03	2.195E-03	2.703E-03
Total (barn)	6.249E+04	5.880E+04	5.636E+04	5.455E+04

Y. Fukaya:

Self-shielding Effect of Double Heterogeneity for Plutonium Burner HTGR Design

Core geometry for horizontal direction

Core geometry for axitial direction
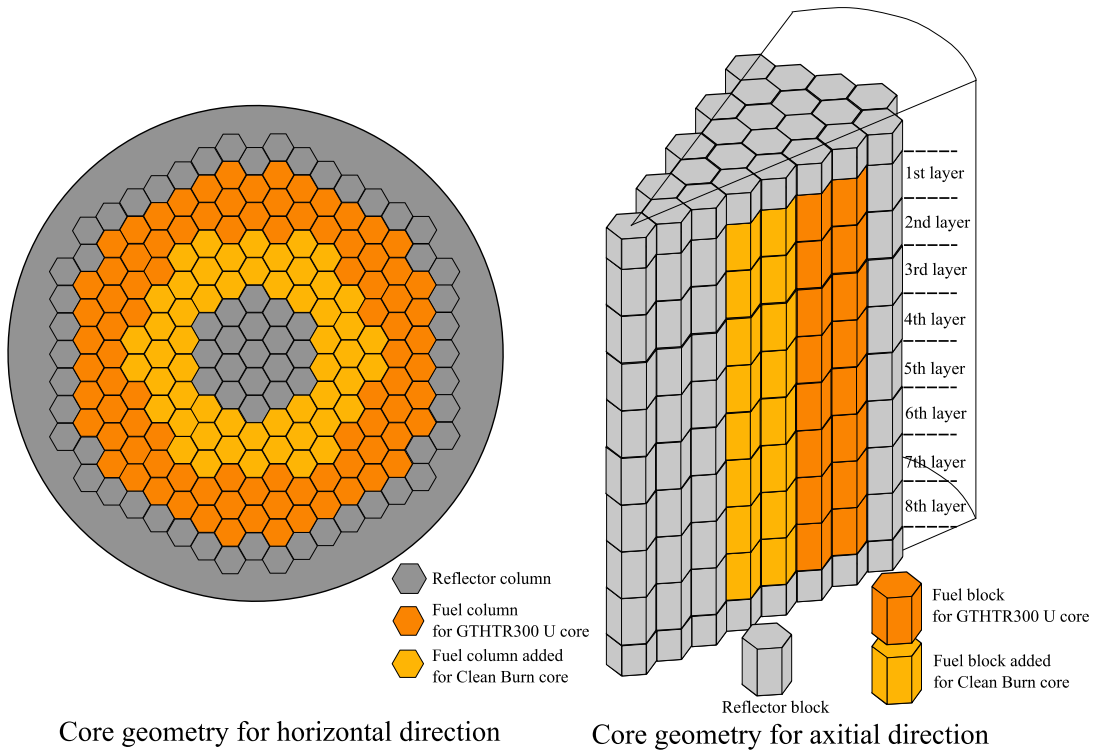
Fig. 1 Core geometry of plutonium burner HTGR

Y. Fukaya:

Self-shielding Effect of Double Heterogeneity for Plutonium Burner HTGR Design
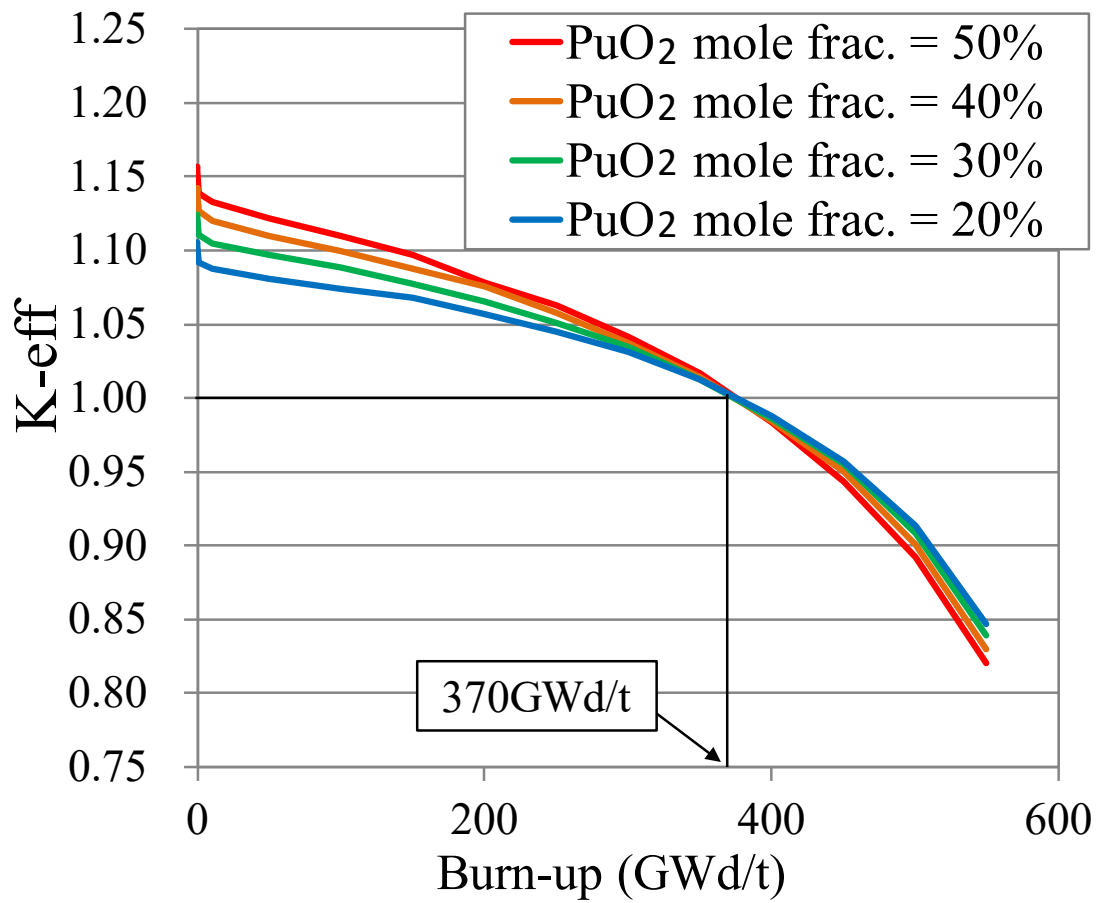
* Statistical error is negligible.

Fig. 2 Excess reactivity suppression by fuel dilution (Fukaya et. al, 2014)

Y. Fukaya:

Self-shielding Effect of Double Heterogeneity for Plutonium Burner HTGR Design

Fuel block pitch: 40.5cm
Fuel cell pitch: 4.7cm
Graphite shaft radius: 0.45cm
Fuel compact radius: 1.20cm
Graphite coating radius: 1.30cm
Coolant hole radius: 1.95cm

Coated fuel particle (CFP)

Outer PyC rayer
Thickness: 40μm
SiC rayer
Thickness: 35μm
Inner PyC rayer
Thickness: 35μm
Buffer rayer
Thickness:150μm
Fuel kernel
Radius: 150μm

Distribution of CFP is determined by statistical geometry model for MVP calculation.

Fuel compact

Ring1
Ring2
Ring3

Shell1
Shell2
Shell3

Graphite coating
Fuel compact
Graphite shaft

Fuel block

Fuel rod

Region division

Fig. 3 Calculation model of MVP code to observe the heterogeneity

and double heterogeneity effect

Y. Fukaya:

Self-shielding Effect of Double Heterogeneity for Plutonium Burner HTGR Design

30

Fuel block pitch: 40.5cm
Fuel cell pitch: 4.7cm
Graphite shaft radius: 0.45cm
Fuel compact radius: 1.20cm
Graphite coating radius: 1.30cm
Coolant hole radius: 1.95cm

Coated fuel particle (CFP)

Outer PyC rayer
  Thickness: 40μm
SiC rayer
  Thickness: 35μm
Inner PyC rayer
  Thickness: 35μm
Buffer rayer
  Thickness:150μm
Fuel kernel
  Radius: 150μm

Fuel lump (Kernel)
Moderator
(Matrix and coating layer)

Fuel compact

Graphite coating
Fuel compact
Graphite shaft

Fuel block   Fuel rod   Microscopic cell

Fig. 4 Calculation model of MOSRA-SRAC code

Y. Fukaya:

Self-shielding Effect of Double Heterogeneity for Plutonium Burner HTGR Design
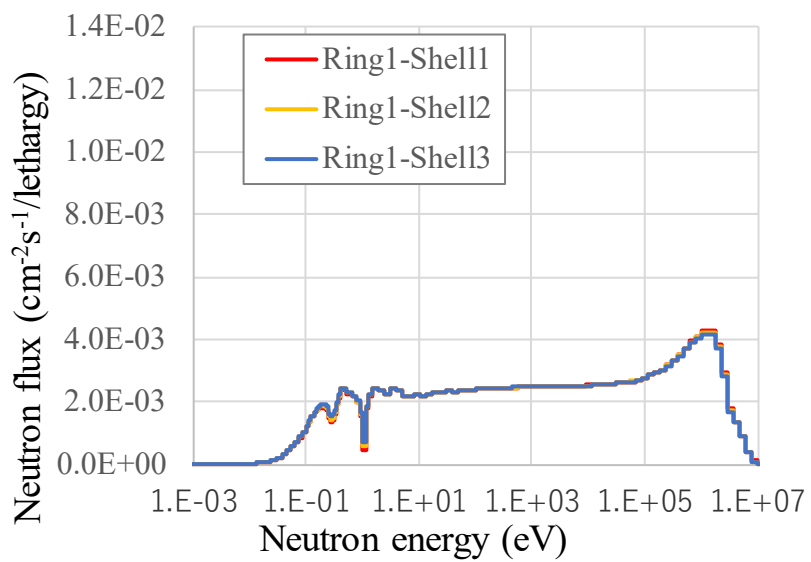
Fig. 5 Neutron flux in fuel kernel in ring1 region at BOL

Y. Fukaya:

Self-shielding Effect of Double Heterogeneity for Plutonium Burner HTGR Design
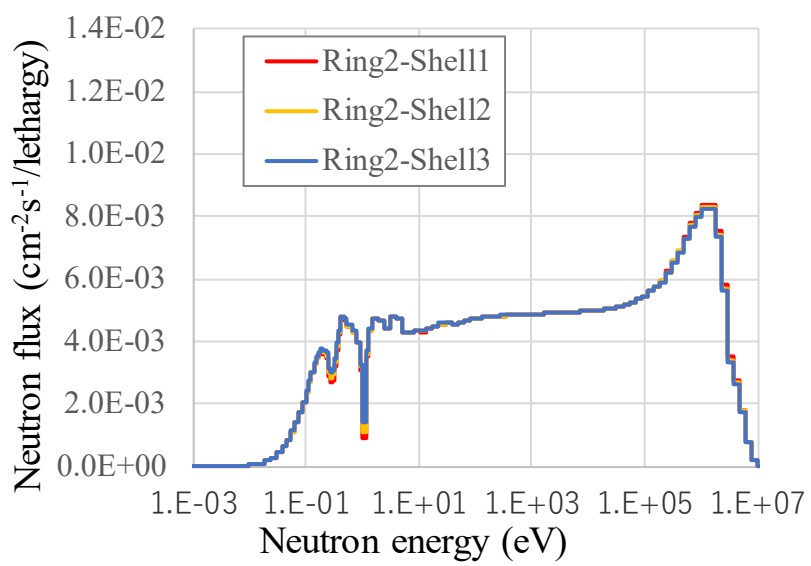
Fig. 6 Neutron flux in fuel kernel in ring2 region at BOL

Y. Fukaya:

Self-shielding Effect of Double Heterogeneity for Plutonium Burner HTGR Design
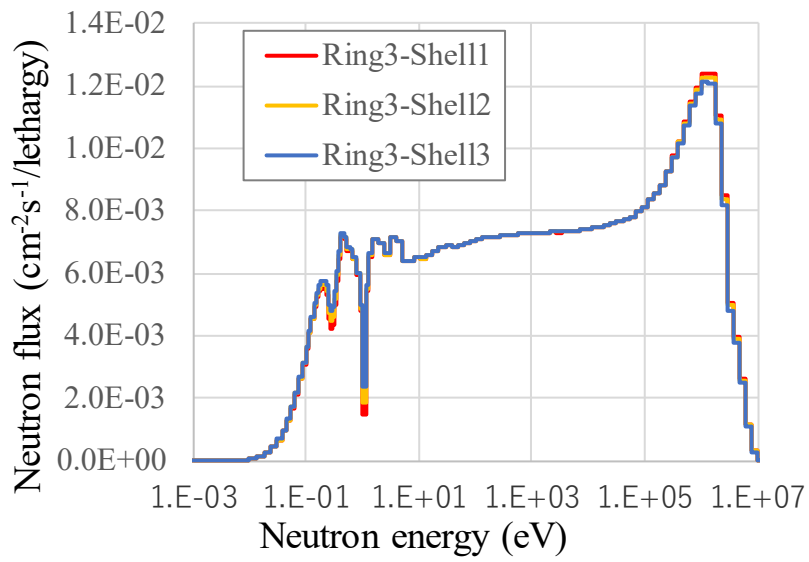
Fig. 7 Neutron flux in fuel kernel in ring3 region at BOL

Y. Fukaya:

Self-shielding Effect of Double Heterogeneity for Plutonium Burner HTGR Design
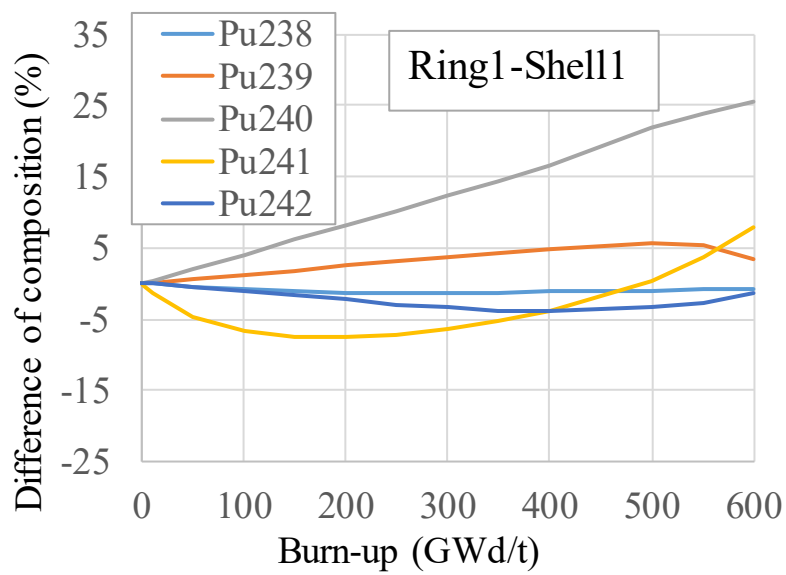
Fig. 8 Difference of burn-up composition in ring1-shell1 region

from that of one-region model

Y. Fukaya:

Self-shielding Effect of Double Heterogeneity for Plutonium Burner HTGR Design
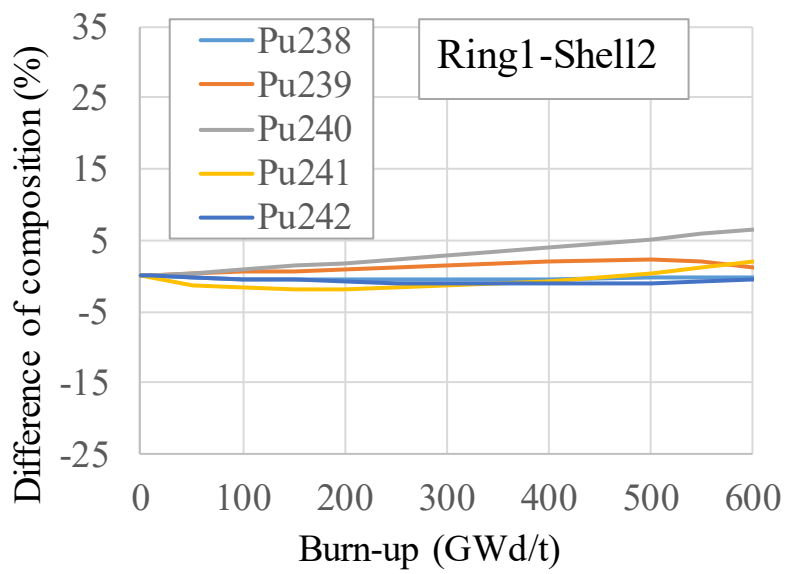
Fig. 9 Difference of burn-up composition in ring1-shell2 region

      from that of one-region model

Y. Fukaya:

Self-shielding Effect of Double Heterogeneity for Plutonium Burner HTGR Design
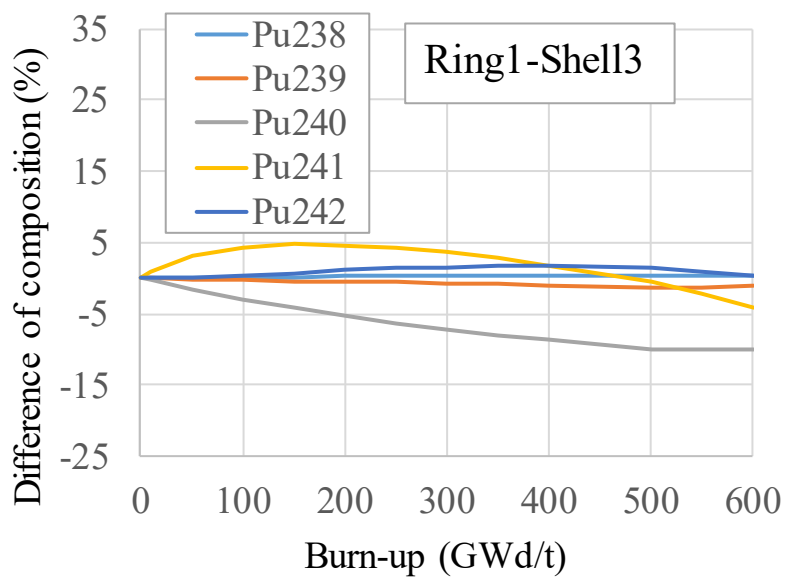
Fig. 10 Difference of burn-up composition in ring1-shell3 region

from that of one-region model

Y. Fukaya:

Self-shielding Effect of Double Heterogeneity for Plutonium Burner HTGR Design
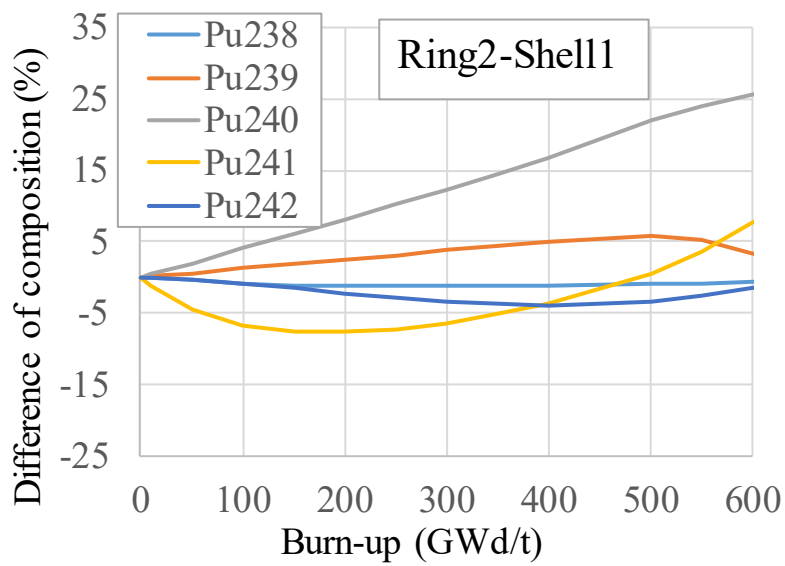
Fig. 11 Difference of burn-up composition in ring2-shell1 region

from that of one-region model

Y. Fukaya:

Self-shielding Effect of Double Heterogeneity for Plutonium Burner HTGR Design
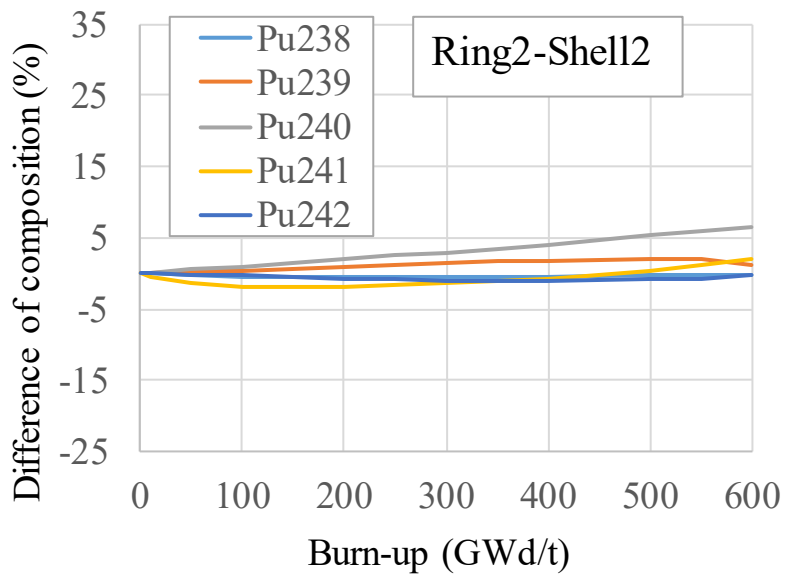
Fig. 12 Difference of burn-up composition in ring2-shell2 region

from that of one-region model

Y. Fukaya:

Self-shielding Effect of Double Heterogeneity for Plutonium Burner HTGR Design
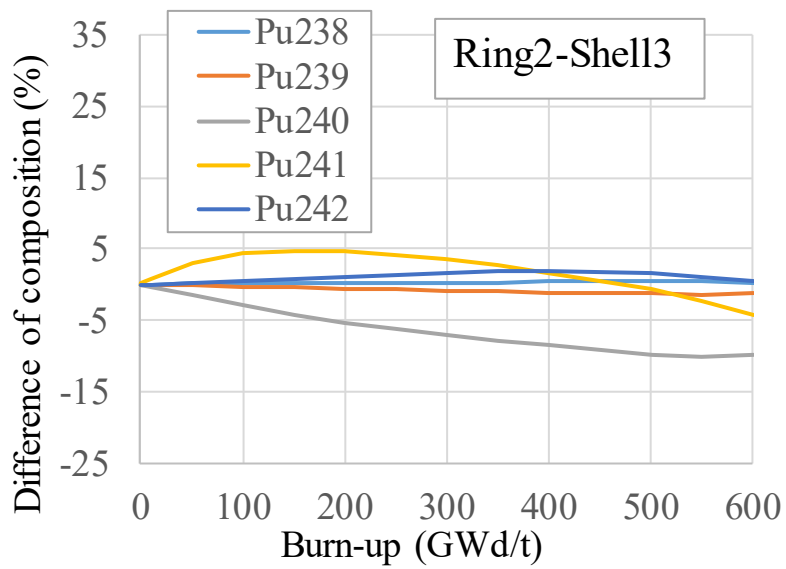
Fig. 13 Difference of burn-up composition in ring2-shell3 region

   from that of one-region model

Y. Fukaya:

Self-shielding Effect of Double Heterogeneity for Plutonium Burner HTGR Design
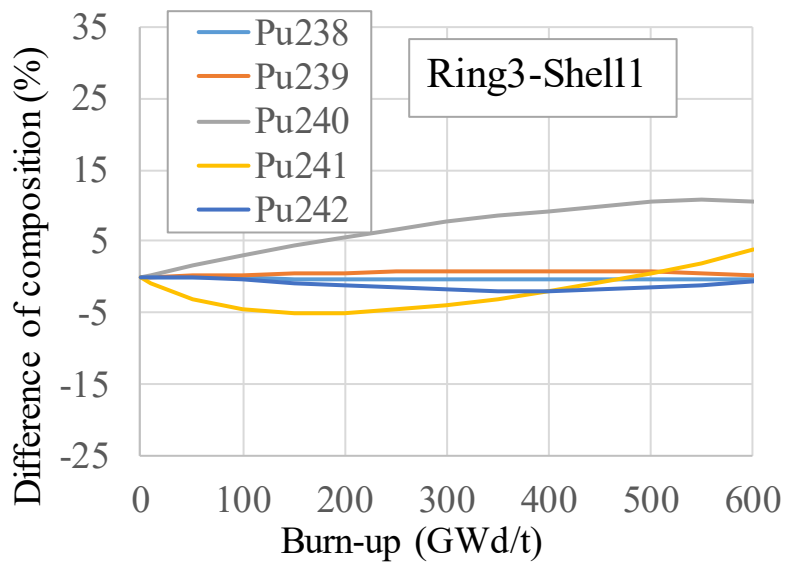
Fig. 14 Difference of burn-up composition in ring3-shell1 region

from that of one-region model

Y. Fukaya:

Self-shielding Effect of Double Heterogeneity for Plutonium Burner HTGR Design
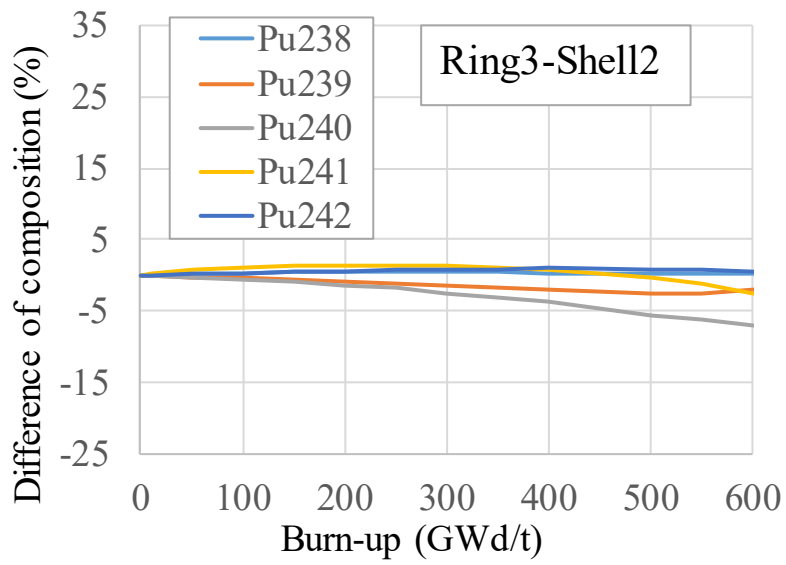
Fig. 15 Difference of burn-up composition in ring3-shell2 region

from that of one-region model

Y. Fukaya:

Self-shielding Effect of Double Heterogeneity for Plutonium Burner HTGR Design
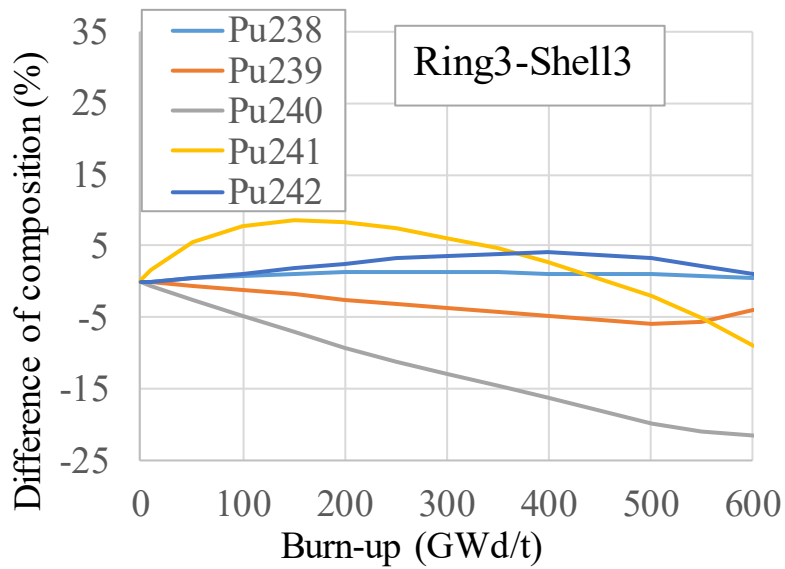
Fig. 16 Difference of burn-up composition in ring3-shell3 region

from that of one-region model

Y. Fukaya:

Self-shielding Effect of Double Heterogeneity for Plutonium Burner HTGR Design
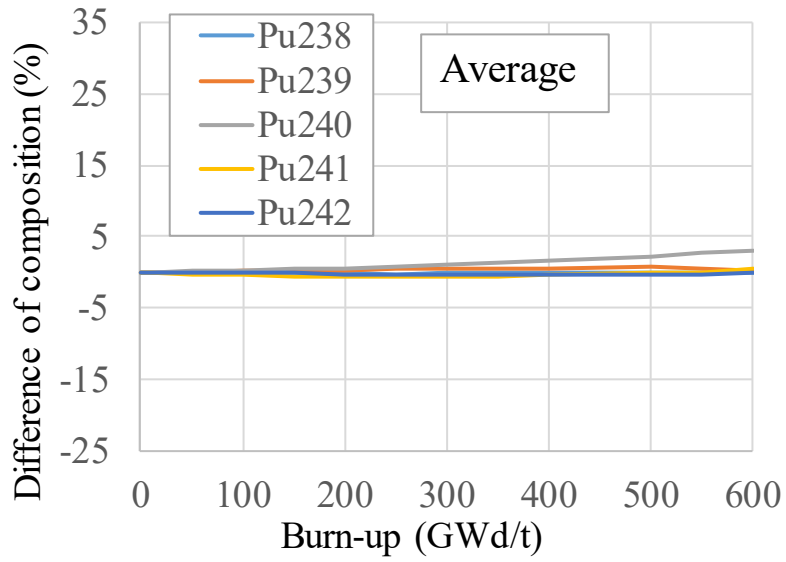
Fig. 17 Difference of burn-up composition of region averaged

from that of one-region model

Y. Fukaya:

Self-shielding Effect of Double Heterogeneity for Plutonium Burner HTGR Design
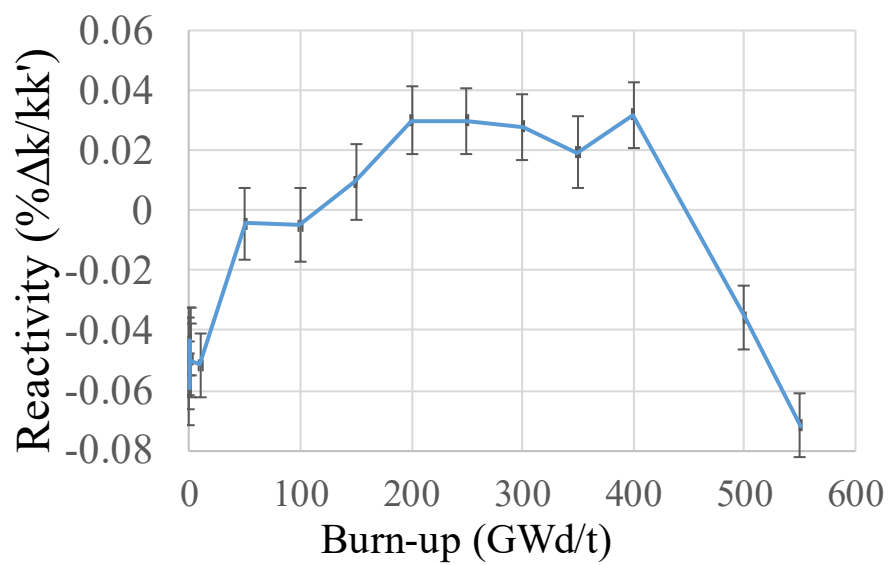
Fig. 18 Reactivity difference between multi-region model and one-region model

Y. Fukaya:

Self-shielding Effect of Double Heterogeneity for Plutonium Burner HTGR Design
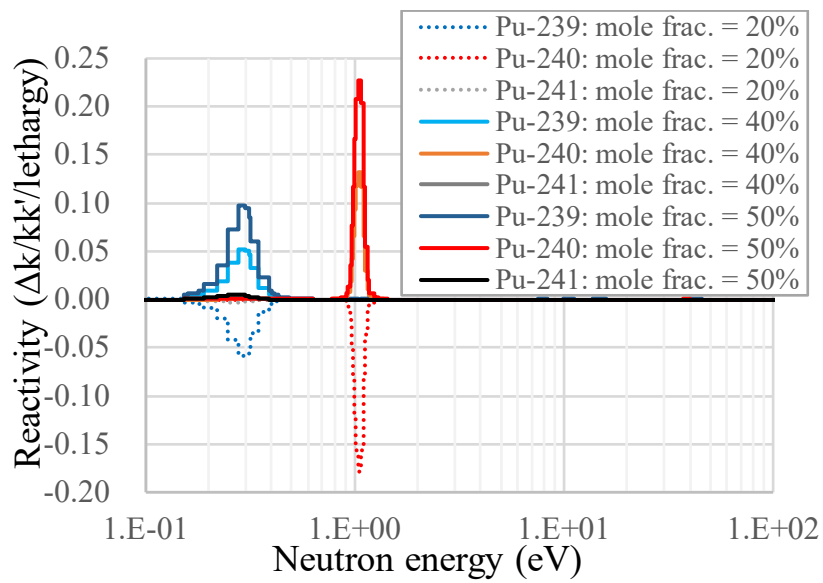
Fig. 19 Absorption reactivity from the mole fraction of 30 % case for each nuclide at BOL

Y. Fukaya:

Self-shielding Effect of Double Heterogeneity for Plutonium Burner HTGR Design
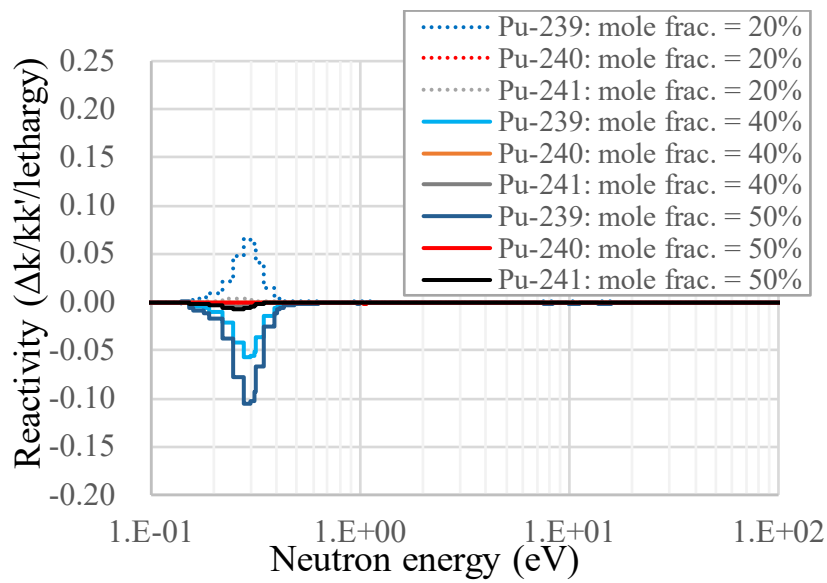
Fig. 20 Fission reactivity from the mole fraction of 30 % for each nuclide at BOL

Y. Fukaya:

Self-shielding Effect of Double Heterogeneity for Plutonium Burner HTGR Design
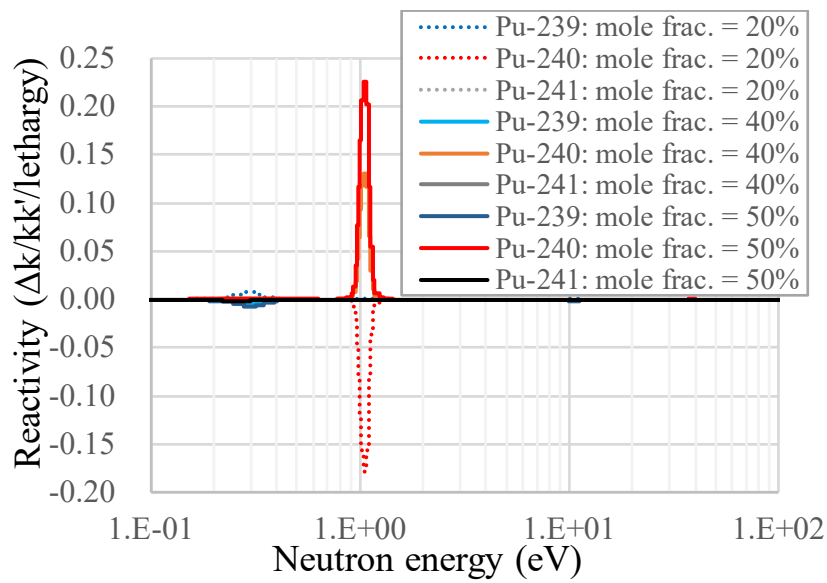
Fig. 21 Total reactivity from the mole fraction of 30 % for each nuclide at BOL

Y. Fukaya:

Self-shielding Effect of Double Heterogeneity for Plutonium Burner HTGR Design
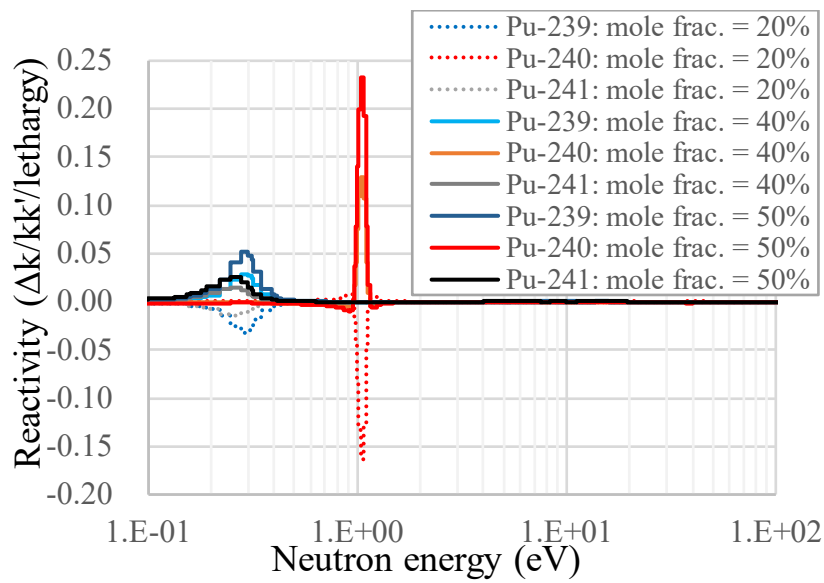
Fig. 22 Absorption reactivity from the mole fraction of 30 % for each nuclide at EOL

Y. Fukaya:

Self-shielding Effect of Double Heterogeneity for Plutonium Burner HTGR Design
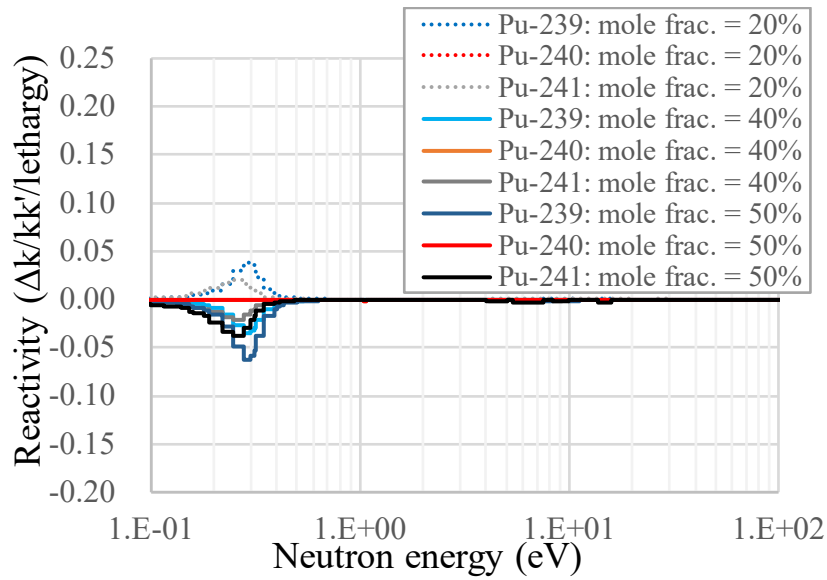
Fig. 23 Fission reactivity from the mole fraction of 30 % for each nuclide at EOL

Y. Fukaya:

Self-shielding Effect of Double Heterogeneity for Plutonium Burner HTGR Design
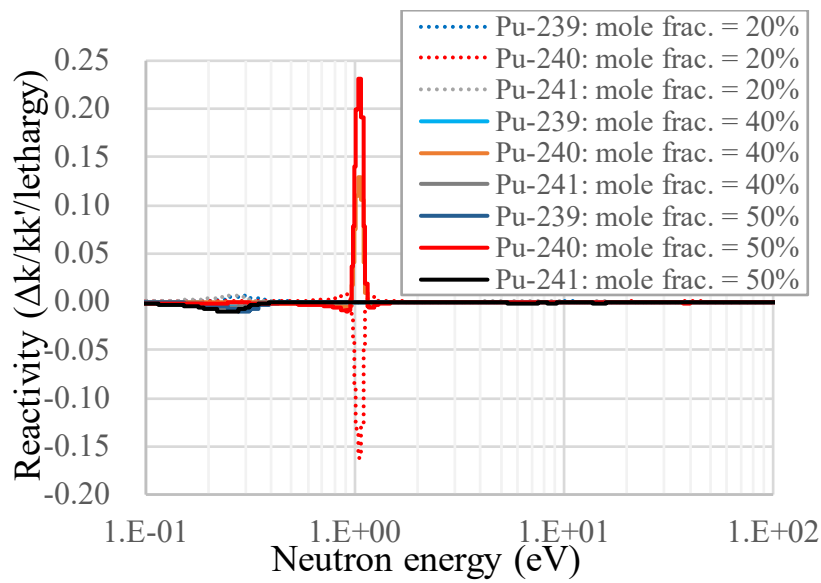
Fig. 24 Total reactivity from the mole fraction of 30 % for each nuclide at EOL

Y. Fukaya:

Self-shielding Effect of Double Heterogeneity for Plutonium Burner HTGR Design
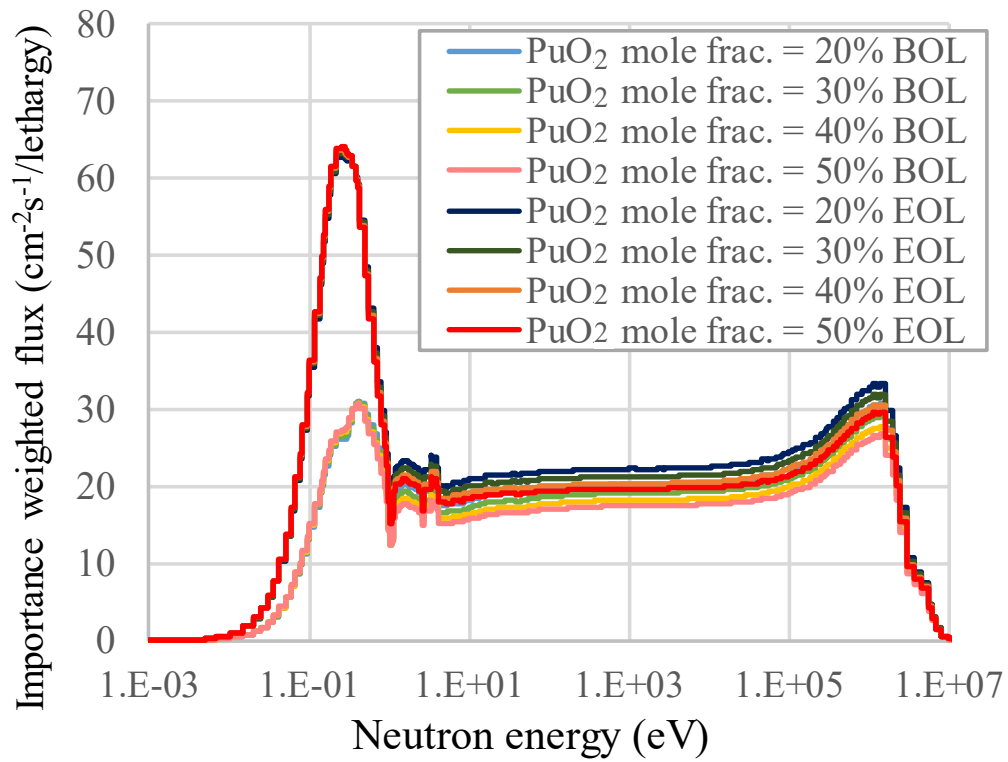
Fig. 25 Importance weighted flux at BOL and EOL

Y. Fukaya:

Self-shielding Effect of Double Heterogeneity for Plutonium Burner HTGR Design